DEM STUDY ON THE MECHANICAL BEHAVIOURS OF METHANE HYDRATE SEDIMENTS: HYDRATE GROWTH PATTERNS AND HYDRATE BONDING STRENGTH

Yanxin YU[*], Yi Pik Cheng
Department of Civil, Environmental and Geomatic Engineering, University College London, Gower Street, London, WC1E 6BT, UNITED KINGDOM

Xiaomin XU, Kenichi SOGA
Geotechnical and Environmental Research Group, Department of Engineering, University of Cambridge, Trumpington Street, Cambridge, CB2 1PZ, UNITED KINGDOM

ABSTRACT

Natural methane hydrate soil sediments attract worldwide interest, as there is huge commercial potential in the immense global deposits of natural gas hydrate that lies under deep seabeds and permafrost regions. However, the geomechanical behaviour of methane hydrate soil is poorly understood. In this study, Discrete Element Method (DEM) was employed to provide insights into the mechanical behaviour of hydrate-bearing sediments with different hydrate patterns in the pores: the pore-filling case and the cementation case. A series of drained triaxial compressional tests were performed, and the results were analyzed in terms of stress-strain response and volumetric response. In both pore-filling and cementation cases, the presence of hydrates caused an increase in the strength and dilative tendency of the simulated hydrate-bearing soil samples, and the strength and dilation both increased with hydrate saturation (or amount of hydrates in the pores). In addition, at the same hydrate saturation, the cementation case showed higher values of strength and dilation than the pore-filling case. In the cementation case, two typical hydrate growth patterns were considered: soil surface coating (hydrates form around the grain surface) and soil-soil contact gathering (hydrates preferentially form at the grain contacts). Results showed that hydrate growth patterns greatly influenced the mechanical behaviour of the simulated hydrate-bearing samples, especially when the bonding strength and hydrate saturation were increased. In both patterns, strength and dilation were enhanced as bonding strength increased, and the enhancement was greater in the soil-soil contact model than in the soil surface gathering model. At high hydrate saturation, as bonding strength increased, a larger axial strain was needed to reach the peak strength, and the development of dilation was delayed.

Keywords: methane hydrate soil, hydrate saturation, pore-filling, cementation, bonding strength, hydrate growth pattern

NOMENCLATURE

D	Particle diameter [mm]	E_c	Elastic modulus [MPa]
D_{50}	Average particle diameter [mm]	E_{c-hyd}/E_{c-soil}	Hydrate-soil elastic modulus ratio
dH	Axial displacement of sample [mm]	H_0	Initial sample height [mm]
dV	Volume change of sample [mm^3]	k_n	Normal contact stiffness [N/m]
		k_s	Shear contact stiffness [N/m]

---
[*] Corresponding author: Phone: +44 20 7679 4407 E-mail: yanxin.yu.10@ucl.ac.uk

$k_{n\text{-hyd}}/k_{n\text{-soil}}(D_{50})$ Hydrate-soil contact stiffness ratio

$k_{n\text{-wall}}$ Normal contact stiffness of wall [N/m]

$k_{s\text{-wall}}$ Shear contact stiffness of wall [N/m]

S_h Saturation of hydrate [%]

V_0 Initial sample volume [mm^3]

μ Inter-particle friction coefficient

μ^{wall} Friction coefficient of wall

ρ Density [kg/m^3]

ε_a Axial strain [%]

ε_v Volumetric strain [%]

σ'_a Effective axial stress [MPa]

σ'_c Effective confining stress [MPa]

σ'_d Effective deviatoric stress [MPa]

σ'_r Effective radial stress [MPa]

INTRODUCTION

Methane hydrate develops in the pores of soil sediments under deep seabeds and permafrost regions under conditions of low temperature and high pressure. These highly compacted methane hydrate soil sediments with immense worldwide deposits have attracted interest as a potential energy resource, which can be extracted by extracting methane gas from hydrate-bearing sediment dissociation, as methane gas is the predominant element of natural gas. However, the extraction of methane gas from the hydrate-bearing sediments also has an impact on geotechnical issues, such as sediment layer instability and wellbore collapse. However, this geomechanical behaviour is poorly understood, particularly in regards to the exploitation process, and further scientific research is needed.

The growth of hydrates in the pores of soil governs the complex response of hydrate-bearing soil to the applied loads and deformations[1][2]. Hence, it is challenging to understand the behaviour of the hydrate-bearing soil, which stands as a special kind of granular material. Apart from the extensive laboratory investigation[1][3][4], many researchers have conducted numerical simulations to study the mechanical behaviour of the hydrate-bearing soil, as it is difficult for lab studies to control the formation, distribution and saturation of the hydrate.

Discrete Element Method (DEM) is a numerical method that models granular materials by explicitly considering their true particulate nature[5]. In this paper, virtual triaxial compression tests were performed using DEM to provide an insight into the mechanical behaviour of hydrate-bearing soil. The discrete element code PFC^{3D} 4.0 was used[6].

In most of the past DEM studies[7][8][9][10], DEM was applied to simulate one hydrate distribution pattern. There was not a consistent DEM model for the comprehensive comparisons among the various hydrate distribution patterns. Therefore, in this paper, two typical types of microscopic hydrate distribution patterns inside soil pores were studied: the pore-filling model and the cementation model. By changing the amount of hydrates in the pores, the hydrate saturation effect was discussed, and the two hydrate distribution patterns were compared in terms of stress-strain response and volumetric response.

PORE-FILLING AND CEMENTATION MODELS

As shown in Figure 1, in the pore-filling model, hydrates nucleate on sediment grain boundaries and grow freely into pore spaces without bridging two or more particles together[1][7][9]. In the cementation model, however, hydrates nucleate at intergranular contacts and soil surfaces, and the existing soil skeleton structure is cemented by the hydrates, while the soil-soil (s-s) contacts are not bonded[1][11].
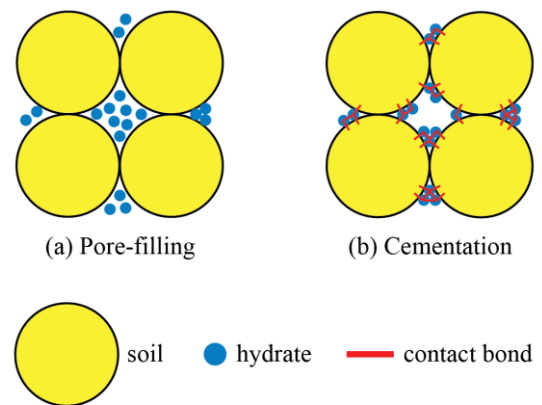

Figure 1 Pore-scale hydrate distribution patterns of hydrate-bearing sediments: (a) pore-filling, (b) cementation

In the cementation model, the hydrate growth patterns could govern the sediment's mechanical

behaviour. Hence, two typical hydrate growth patterns of the cementation model were considered: soil surface coating (hydrates accumulating at grain surface) and soil-soil contact gathering (hydrates aggregating near the grain contacts). DEM simulations were conducted on these two cementation hydrate growth patterns with various bonding strength in order not only to compare the two patterns, but also to study the bonding strength effect.

Sample preparation

The parameters for DEM sample preparation are summarized in Table 1[9][11]. The sizes of spherical soil particles followed the principle of Gaussian distribution. There is limited data in the literature providing experimental results around the elastic modulus (E_c) of hydrates[7]. The hydrate-soil elastic modulus ratio ($E_{c\text{-}hyd}/E_{c\text{-}soil}$) was set to 0.1 according to the DEM research of Brugada et al. (2010) [7]. In the DEM study of PFC^{3D}, the normal contact stiffness k_n is proportional to the particle elastic modulus (E_c) and the particle diameter (D) (i.e. $k_n = 2DE_c$). Hence, the hydrate-soil contact stiffness ratio $k_{n\text{-}hyd}/k_{n\text{-}soil}(D_{50})$ was 0.023.

Property	Soil	Methane hydrate
Particle size D (mm) (Gaussian distribution)	0.1-0.25	0.04
Density ρ (kg/m^3)	2600	900
Elastic Modulus E_c (MPa)	286	28.6
Normal contact stiffness k_n (N/m)	$2DE_c$	$2DE_c$
Shear contact stiffness k_s (N/m)	$0.7k_n$	$0.7k_n$
Inter-particle friction μ	0.75	0.75

Table 1. Input parameters used in the DEM model

As shown in Figure 2, the pore-filling model samples were cylinders of 1.75 mm (diameter) × 3.5 mm (height) with a height/diameter ratio of 2:1[9]. It was confined by a frictionless lateral cylindrical wall and with frictionless planar walls at the top and bottom ($\mu^{wall} = 0$). In this study the normal stiffness of the walls was set to be approximately 100 times that of the largest soil particles' normal stiffness ($k_{n\text{-}wall} = 1.5 \times 10^7$ N/m, $k_{s\text{-}wall} = 1.5 \times 10^7$ N/m). A soil sample with an initial porosity of 0.43 was first consolidated to the

isotropic effective stress of 1 MPa, as natural methane hydrate develops under high pressure. Gravity was not applied to the particles. Following this, hydrate particles were generated in the void space of the sample randomly to reach a chosen hydrate saturation (S_h) which refers to the percentage of hydrate volume occupancy in the void space of the pure soil sample, as shown in Figure 2. It should be noted that the hydrate saturation computed here may not be the same as the hydrate saturation measured in the laboratory. This is because soils and hydrates are not spherical particles; it is likely that hydrate saturation was underestimated. Hence, the behaviour observed in this study should be examined qualitatively rather than quantitatively.
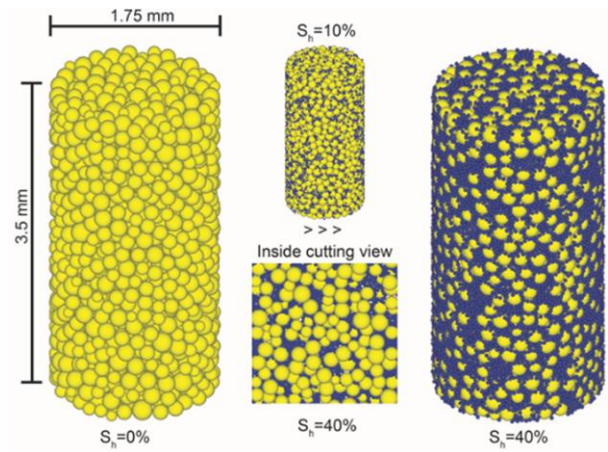

Figure 2 DEM hydrate-bearing soil samples.

The cementation samples were generated using a consistent model[11] which was almost the same as the pore-filling model, but with hydrate particles forming first at the grain contacts, then growing in the pores from these contacts, as well as along the soil surface according to the laboratory observations of Priest et al. (2005)[12]. The hydrate particles were bonded to soil particles as well as other hydrate particles with the normal and shear bonding strength of 5×10^3 N/m^2 (0.005 MPa) using the contact bond model of PFC^{3D}. The soil particles were not bonded together.

Simulation results

After the sample preparation, a series of drained triaxial compression tests were systematically performed at different hydrate saturations using both models. Before the drained triaxial compression tests, the sample was subject to the

effective stress: an isotropic consolidating stress σ'_c = 1MPa. The test was then started by increasing the axial load σ'_a (by moving the top and bottom boundaries at a constant speed) while the servo-controlled lateral pressure was held at the constant confining stress σ'_c, as shown in Figure 3. The axial (vertical) compressive stress was increased by σ'_d, which was termed to deviatoric stress. Thus, the final stress was:

Final axial stress, $\quad \sigma'_a = \sigma'_c + \sigma'_d \quad$ (1)

Final radial stress, $\quad \sigma'_r = \sigma'_c \quad$ (2)
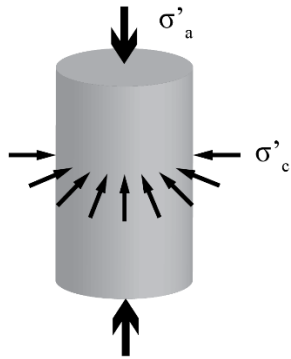
Figure 3 Sketch diagram of triaxial test

Under the confining pressure σ'_c of 1 MPa and a hydrate/soil contact stiffness ratio $k_{n\text{-hyd}}/k_{n\text{-soil}}(D_{50})$ of 0.023, the stress-strain relationships of hydrate-bearing samples are illustrated in Figure 4(a) and Figure 4(b) for the pore-filling model and the cementation model with different hydrate saturations (S_h= 0%, 10%, 20%, 30%, 40%). The history of loading of a sample was recorded by the plots of the deviatoric stress as a function of axial strain, which are defined as:
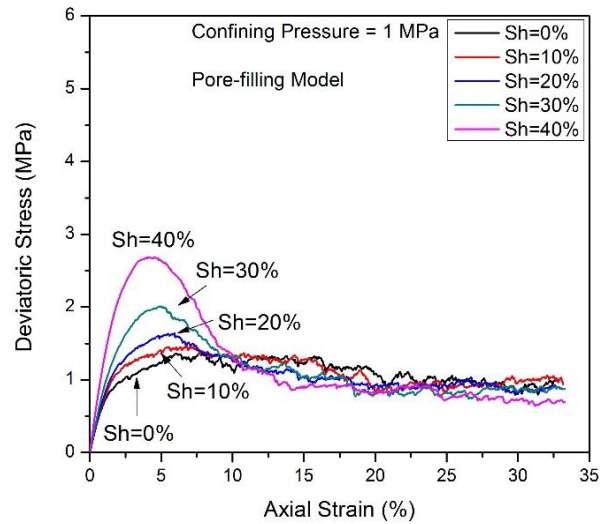
Deviatoric stress, $\quad \sigma'_d = \sigma'_a - \sigma'_r \quad$ (3)

*Axial strain,* $\quad \varepsilon_a = \dfrac{dH}{H_0} \quad$ (4)

where H_0 is the initial sample height before shearing, and dH is the axial displacement of the sample during the triaxial compression test.

Generally, in the triaxial test of the dense hydrate-bearing sample, the stress-strain curve was initially steep, reached a peak point, and then fell to a constant critical state value. In both pore-filling and cementation models, the stiffness and the peak strength (maximum deviatoric stress) increased with hydrate saturation. In the pore-filling samples, the maximum deviatoric stress increased with hydrate saturation, from 1.37 MPa (S_h=0%) to 2.75 MPa (S_h=40%). In the cementation samples, the maximum deviatoric stress increased from 1.37 MPa (S_h=0%) to 5.50 MPa (S_h=40%). Hence, the hardening effect of hydrates were shown in both cases. In the pore-filling model, the strength increased when the hydrate saturation was more than 20%. However, in the cementation model, the strength increased just after there were some hydrates growing in the sediments.

(a) Pore-filling model
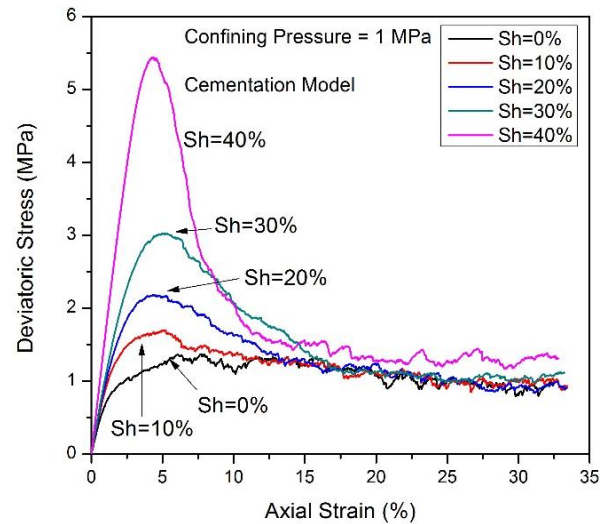
(b) Cementation model

Figure 4 Deviatoric stress as a function of axial strain

However, the rate of peak stress increase with hydrate saturation was influenced by the growth pattern of methane hydrate in the soil pores. At the same hydrate saturation, the elastic stiffness and the peak strength of the pore-filling sample were smaller than those of the cementation sample, as shown in Figure 5. At the low hydrate saturations, hydrates in the pore-filling case did not contribute to the strength of the sediments at the beginning of the triaxial test as hydrates were formed inside the pore space rather than at the soil particles' contacts. The hydrates in the cementation case grew at the soil particle contacts and along the soil particle surfaces, hence hydrate particles contributed to the strength of the soil skeleton during the deformation. At high hydrate saturation, the contribution of hydrates in the pore-filling case became more evident.
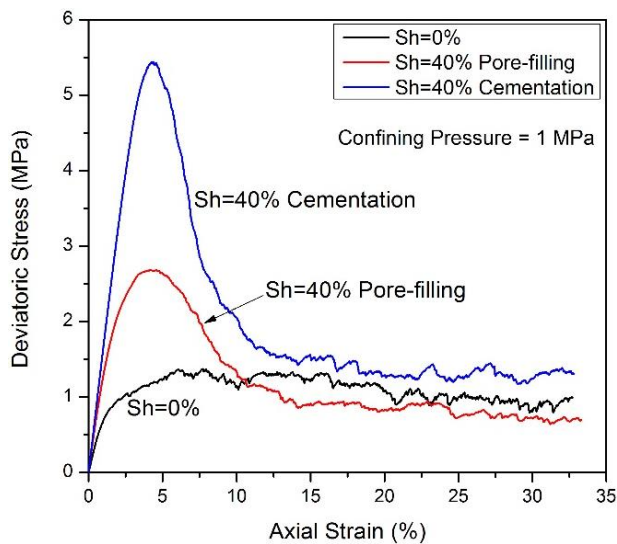

Figure 5 Comparisons of deviatoric stress as a function of axial strain between pore-filling and cementation cases at S_h=40%

Compared to previous experimental and numerical studies[1][3][7][8][10], our interest in this research extended to large strain and critical state behaviour. At large axial strain levels, softening behaviour was observed, and the deviatoric stress at critical state reduced to some constant values. Compared to the S_h=0% sample's critical state shear strength, there was a reduction in the critical state strength of the pore-filling case, as shown in Figure 4(a) and Figure 5. The reduction was more evident at higher hydrate saturations. In the cementation case, on the contrary, the critical state

shear strength at S_h=40% was greater than that at S_h=0%, as shown in Figure 4(b) and Figure 5.

The volumetric strain ε_v refers to the unit change in volume due to a deformation, as defined in Equation (12).

$$\text{Volumetric strain,} \quad \varepsilon_v = \frac{dV}{V_0} \quad (5)$$

where V_0 is the initial sample volume, and dV is the volume change of the sample during the triaxial compression test.

(a) Pore-filling model
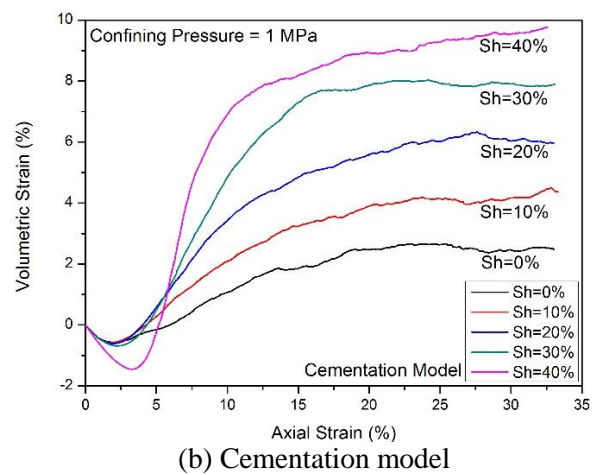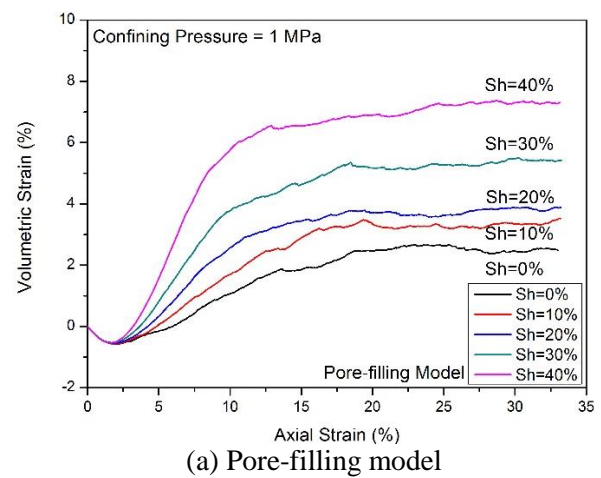

(b) Cementation model

Figure 6 Volumetric strain as a function of axial strain

Figure 6 shows the volumetric strain – axial strain relationships of the samples with different hydrate saturations. The sediments initially showed contractive behaviour, which was followed by a

dilative tendency. In addition, the dilatancy was enhanced by increasing hydrate saturation. The peak contractive values in the pore-filling model were similar at different hydrate saturations, whereas those in the cementation model increased with hydrate saturation. Peak contractive values in the cementation model, particularly at S_h=40%, saw a large number of bonding contacts and a higher occasion of interlocking particles. At the beginning, this made the soil particles immobile relative to each other, and due to the elastic deformation of the particles, caused the sample to compress more. When particles start to move relative to each other, dilation happens and the rate of dilation of the cementation model (see Figure 6(b)) is greater than that of the pore filling model (see Figure 6(a)). At the critical state, the volume of the hydrate-bearing sample became constant, as expected.

CEMENTATION HYDRATE GROWTH PATTERNS

Sample preparation
In the natural cementation hydrate-bearing sediments, hydrates grow along grain surfaces and at grain contacts. The mechanical behaviour could be governed by hydrate growth patterns.

(a) Coating (No bond)

(a') Coating (With bond)

(b) Contact-Gathering (No bond)
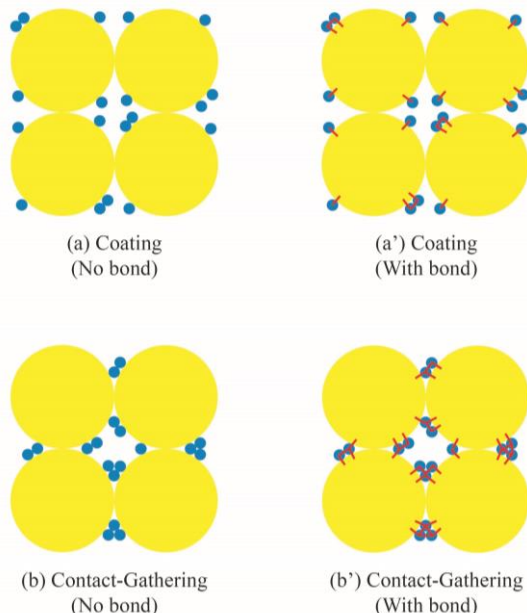
(b') Contact-Gathering (With bond)

Figure 7 Hydrate growth patterns of the cementation model: (a) soil surface coating (b) soil-soil contact gathering

In this study, DEM simulations were performed with samples of two different growth patterns: (i) hydrates placed around grain surfaces ("Coating" in Figure 7(a)) and (ii) hydrates placed near grain contacts ("Contact gathering" in Figure 7(b)). The bonding strength of hydrate-hydrate and hydrate-soil was also varied, as shown in Figure 7(c) and (d).

In order to study the bonding strength effect of the hydrate particles, DEM simulations were conducted on the two cementation hydrate growth patterns at various bonding strengths – 0 MPa (no bond), 0.005 MPa, 0.010 MPa, 0.025 MPa, 0.050 MPa and 0.500 MPa using the contact bond model in PFC^{3D}. The soil particles were not bonded together.

Simulation results

The stress-strain relationships obtained from the drained triaxial compression tests are plotted in Figure 8 and 9, which show deviatoric stress against axial strain, for samples with the coating hydrate pattern and the contact-gathering hydrate pattern at S_h=10% and 30%, with an increase in the bonding strength of the hydrate particles.

As the bonding strength increased, the strength of the hydrate-bearing soil samples was enhanced. Secondly, in the same bonding strength and hydrate saturation conditions, the strength of the soil-soil contact gathering model was larger than that of the soil surface coating model, which can be observed when comparing Figure 8(a) and 8(b) at the low hydrate saturation of 10%. The contact-gathering hydrate particles strengthened the soil skeleton more than the coating hydrate particles by bonding the inter-granular contacts.

In both Figure 8 and 9, as the bonding strength increased, a larger axial strain was needed to reach the peak strength, and the failure was delayed. When the bonding strength was 0.500 MPa, as shown in Figure 8(b) and Figure 9, a large axial strain of 33% was not enough to lead the sample to a failure.

Regarding the volumetric responses of the coating and contact-gathering patterns, the volumetric strain against axial strain was plotted in Figure 10 and 11. In Figure 10, at the hydrate saturation of 10%, a high bonding strength caused a larger

dilation at large axial strains. At high bonding strengths of 0.050 MPa and 0.500 MPa, the dilation of the coating pattern was larger than that of the contact-gathering pattern. This may be because of the interlocking caused by the contact-gathering hydrate particles interacting with high bonding strength restricted grain movements, hence causing limited dilation.
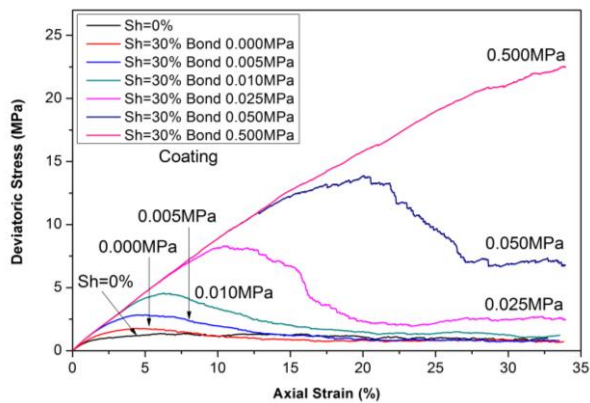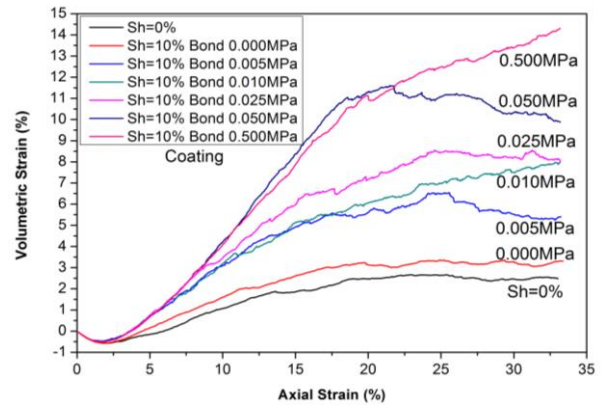

(a) Coating
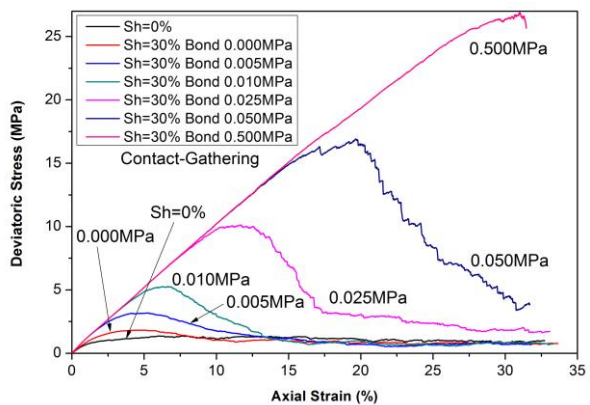
(b) Contact-gathering

Figure 9 Deviatoric stress as a function of axial strain (S_h=30%)

As shown in Figure 11, as hydrate saturation increased, the dilation was enhanced in both hydrate growth patterns. However, when the hydrate saturation increased to 30%, the dilation of the coating pattern was smaller than that of the contact-gathering pattern for a given bonding strength. As discussed before, when the bonding strength is very large, grains could not move and the deformation was controlled by the elastic deformation of the particles themselves. However, when the grains do start to move relative to each other, and as the bonds were broken, dilation

started to occur and big clusters of bonded particles caused larger dilation, especially using the contact-gathering pattern. It appears that hydrate particles gathered at the grain contacts tend to form big hydrate clusters, which in turn gives more dilation.
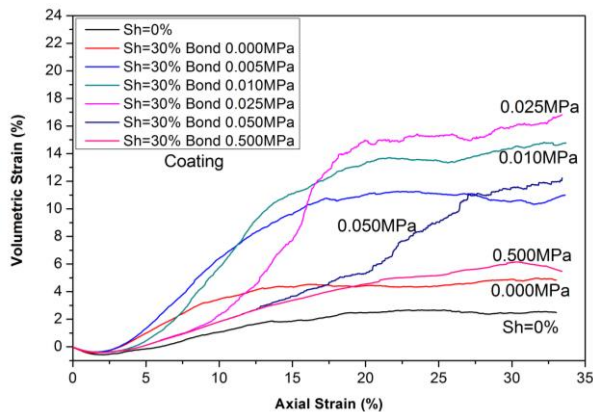

(a) Coating
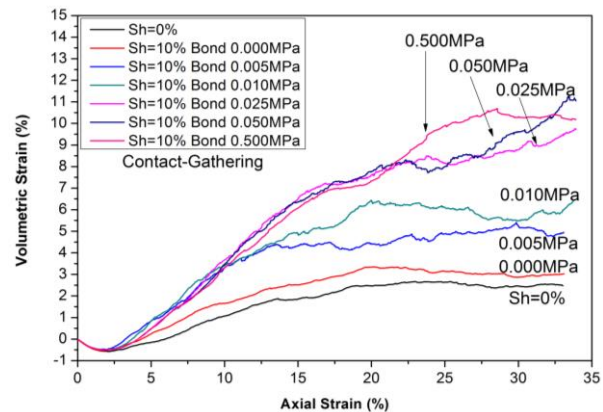
(b) Contact-gathering

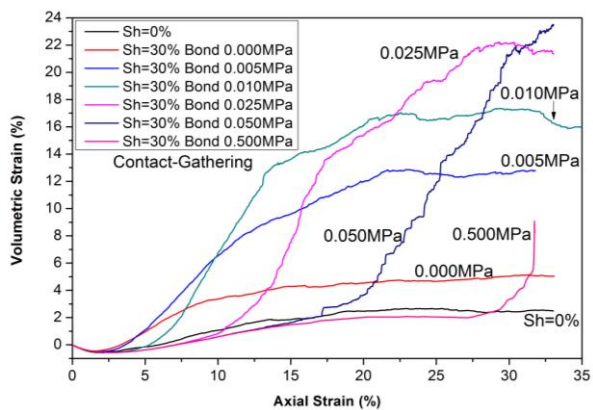Figure 10 Volumetric strain as a function of axial strain (S_h=10%)

CONCLUSIONS

In this paper, Discrete Element Method (DEM) was employed to provide insights into the mechanical behaviour of hydrate-bearing sediments with different hydrate patterns in the pores (pore-filling versus cementation). For the cementation case, two hydrate growth patterns (hydrates coating around grain surface versus hydrates gathering near grain contacts) were used, and bond strengths varied. A series of drained triaxial compressional tests were systematically simulated, and comprehensive analyses in terms of stress-strain response and volumetric response were conducted.

In both pore-filling and cementation models, the presence of hydrates caused an increase in the strength and dilation of the hydrate-bearing soil. For a given hydrate saturation, the cementation model showed higher strength and dilation values than the pore-filling model.

(a) Coating

(b) Contact-gathering

Figure 11 Volumetric strain as a function of axial strain (S_h=30%)

The hydrate growth patterns in the cementation model greatly influenced the mechanical behaviour of the hydrate-bearing sediments, especially when the bonding strength and hydrate saturation were increased. For a given bonding strength and hydrate saturation, the strength of a sample with hydrates gathering near grain contacts was greater than that of a sample with hydrates coating around the grain surface. When a high bond strength was assigned, the deformation at small strains was controlled by the deformation of the particles themselves, and the dilation was delayed. When grains started to move relative to each other by bond breakage, samples exhibited dilation, with a greater dilation being observed in the grain coating case compared with the contact gathering case.

REFERENCES
[1] Soga K, Lee S L, Ng M Y A and Klar A. *Characterisation and engineering properties of methane hydrate soils*. Characterisation and Engineering Properties of Natural Soils, Taylor and Francis, 2006 Vol. 4, pp.2591-2642.
[2] Waite W F, Santamarina J C, Cortes D D, Dugan B, et al., *Physical properties of hydrate-bearing soils*. Review of Geophysics, 2009. 47(RG4), 3－41.
[3] Masui A, Haneda H, Ogata Y and Aoki K. *The effect of saturation degree of methane hydrate on the shear strength of synthetic methane hydrate sediments*. Proceedings of the 5th Int. Conf. on Gas Hydrates. June 13-16, 2005, Trondheim, Norway. Paper No. 2037.
[4] Hyodo M, Yoneda J, Nakata Y and Yoshimoto N. *Strength and dissociation property of methane hydrate bearing sand. Proceedings of the 7th International Conference on Gas Hydrates (ICGH2011)*, Edinburgh, Scotland, United Kingdom, July 17-21, 2011.
[5] Cheng Y P, Nakata Y and Bolton M D. *Discrete element simulation of crushable soil.* Geotechnique, 2003, 53, No. 7, 633-641.
[6] Itasca, *PFC3D: Particle flow code. User's guide version 4.0*, Minneapolis, USA, 2008.
[7] Brugada J, Cheng Y P, Soga K and Santamarina J C, *Discrete element modelling of geomechanical behaviour of methane hydrate soils with pore-filling hydrate distribution*, Granular Matter, 2010, vol. 12, no. 5, pp. 517-525.
[8] Jung J W, Santamarina J C and Soga K. *Stress-Strain Response of Hydrate-Bearing Sands: Numerical Study Using DEM Simulations*. Journal of Geophysical Research - Solid Earth, 2012, Vol. 117, B04202, 12 pp..

[9] Yu Y, Cheng Y P and Soga K, *Mechanical behaviour of methane hydrate soil sediments using Discrete Element Method: Pore-filling hydrate distribution. The proceedings of the International Symposium on Discrete Element Modelling of Particulate Media*, Birmingham, RSC Publishing, March 2012, pp. 264-270.

[10] Jiang M J, Sun Y G, Yang Q J. *A simple distinct element modelling of the mechanical behaviour of methane hydrate-bearing sediments in deep seabed*, Granular Matter, 2013, 15: 209-220.

[11] Yu Y, Xu X, Cheng Y P, and Soga K, *Study on small-strain behaviours of methane hydrate sandy sediments using discrete element method, Powders and Grains 2013*, AIP Conf. Proc. 1542, 555-558.

[12] Priest J A, Best A I and Clayton C R I. *A laboratory investigation into the seismic velocities of methane gas hydrate-bearing sand*, Journal of Geophysical Research, 2005, vol. 110.